Available online at www.sciencedirect.com

ScienceDirect

IFAC PapersOnLine 52-21 (2019) 14–20

Effects of Flexible Propulsors on Hydrodynamic Forces

Hisham M. Shehata * **Muhammad R. Hajj** **
Craig A. Woolsey *** **Saad Ragab** *

* *Biomedical Engineering and Mechanics, Virginia Tech*
Blacksburg, VA 24061 USA (E-mail: {hshehata, ragab}@vt.edu).
** *Civil, Env., & Ocean Engineering, Stevens Institute of Technology*
Hoboken, NJ 07030 USA (E-mail: mhajj@stevens.edu)
*** *Aerospace & Ocean Engineering, Virginia Tech*
Blacksburg, VA 24061 USA (E-mail: cwoolsey@vt.edu)

Abstract: We present experimental measurements of forward forces and external torques generated during forced oscillations of a tail on a fish-like body. The experiments were performed in a towing basin. Three panels having different flexural rigidity were tested over a range of oscillatory frequencies and leading edge amplitudes at 0 m/s and 0.35 m/s. The results show that tail panel flexibility enhances thrust production and thrust-to-input power ratios, with propulsive efficiencies reaching up to 45%.

Keywords: Hydrodynamics, thrust, propulsive efficiency, biolocomotion, towing basin

1. INTRODUCTION

Interest in the generation of propulsive forces by biological creatures is inspired by their impressive structural and kinematic capabilities, and their morphological adaptations. The current research and design of fish-like locomotion devices primarily focus on demonstration of "proof of concept", yet its routine application acquires few strategies and hydrodynamic principles to inform the design of efficient biomimetic propulsion and control systems. Particularly, the interest in the role of flexibility in propulsive performance for biologically inspired underwater vehicles has been rising.

Incorporating flexibility on swimming devices has been explored as a mechanism to improve aerodynamic and hydrodynamic performance (Shyy et al., 2005; Dewey et al., 2013; Quinn et al., 2014; Ghommem et al., 2014). Extensive theoretical, numerical and experimental work on the flapping of rigid foils have shown optimum thrust over ranges of Strouhal numbers, a non-dimensional frequency, of $St = 0.25 - 0.4$ consistent with the range observed in nature (Anderson et al., 1998; Triantafyllou et al., 1993). Further attention has been recently given to flexible rectangular panels as propulsors where material stiffness, aspect ratio, and swimming speeds are the primary driving parameters for achieving higher propulsive efficiency (Lauder and Madden, 2007). Additionally, most literature shows that propulsive performance of heaving and pitching plates depends strongly on structural resonance. While most experimental studies (Quinn et al., 2014; Prempraneerach et al., 2003) report that actuation within 10% of the structures resonant frequency achieved the highest Froude (propulsive) efficiencies, others have found the highest efficiencies within 30-50% of the resonant frequencies (Kang et al., 2011a). Incorporating flexibility into the pitching mechanism on wings of micro-air vehicles (MAVs) has also been shown to have a profound impact on propulsive efficiency, exhibiting a band of frequencies over which flexible panels produce more thrust than rigid panels (Heathcote and Gursul, 2007).

Under certain swimming parameters, the motion created by an oscillating foil reverses the rotational direction of the vortex shedding in the wake. This results in the formation of the "reverse von-Kármán street". The pattern formed by the vortices in the wake induces a jet-like push in the direction of the mean flow (Eloy, 2012; Koochesfahani., 1989). The unsteady vortex control can additionally generate higher lift coefficients that can be used for maneuvering, and the recapture of vortical energy from incoming flow can be manipulated to result in minimal energy utilization by the system (Triantafyllou et al., 1991).

The purpose of this work is to provide detailed measurements of the thrust forces and servo torques, and determine the effect of fish tail flexibility on the overall propulsive performance. The experiments were conducted with and without forward towing speed to compare the hydrodynamic performance between the two scenarios. The work also aims to provide data that can be used to validate computational tools.

2. EXPERIMENTAL SYSTEM

2.1 Prototype Design And Model Setup

The physical device used for the experimentation is shown in figure 1. The forebody and the tail piece were 3-D printed using Abs-M30 material. The forebody of the swimming prototype (light blue part in figures 1 (b) and 1 (c)) has the shape of a NACA-0024 airfoil truncated at 75% of its chord length. The rest of the body consists of an attached tailpiece (the purple piece in figure 1)

10.1016/j.ifacol.2019.12.276

that is connected to the back end of the forebody by a hinge that allows for smooth rotation. The tailpiece itself is semi-elliptical in shape that extends into a rectangular planform with two drill holes and enough spacing to fit in panels of any shape, length, and material. Three tail panels were in the current experiment. Their dimensions and material properties are listed in table 1. The total length of the forebody from its leading edge is 45 cm with the tailpiece and 41 cm without the tailpiece. The height of the prototype is 10 cm.

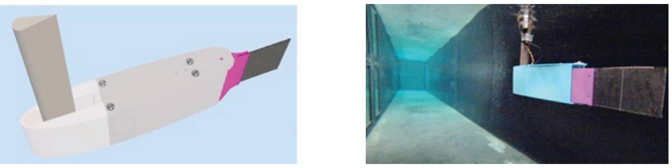

(a)CAD drawing of the model (b)Swimming model

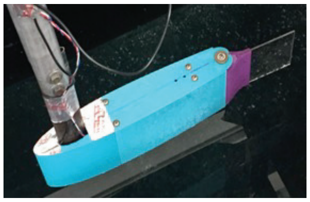

(c)Assembled model

Fig. 1. Physical Device used for experimentation

The forebody compartment contains the waterproof L-shaped sting balance with wires running from the strain gauge up to the onboard box converter. The aft compartment (tailpiece) contains the servo motor. The tail joint is actuated using a waterproof Hitec WPHS-55 high torque high voltage servo to provide the oscillatory motion with a range of ±20° relative to the hinge point. Figure 2 shows a transparent view of the swimming device.

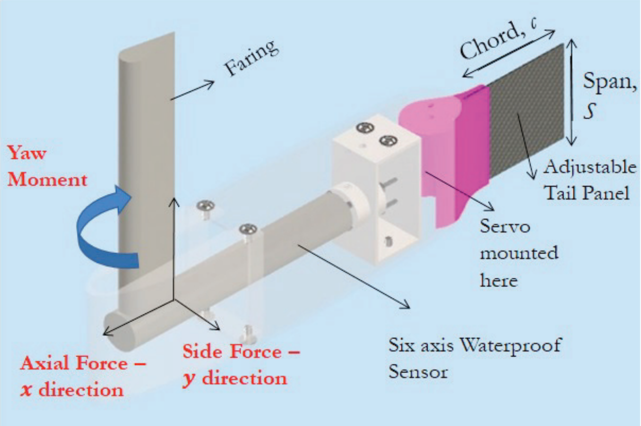

Fig. 2. CAD model - transparent view

2.2 Test facility - Towing basin

The experiments were conducted in the towing basin located in Norris Hall at Virginia Tech, shown in figure 3. The towing basin is 30 m long, 1.8 m wide and 1.2 m deep. The sting holding the prototype was placed at full extension making the distance between the top surface of the prototype roughly 0.31 m under the surface of the water, and 0.76 m away from the end walls. The measurements were obtained by towing the device by an instrumented towing carriage driven by a 400 VDC motor, and capable of reaching a maximum speed of 3 m/s.

Fig. 3. From left to right: Towing carriage, control panel unit, and towing tank

2.3 Data Acquisition

The load cell used is a sting balance SB-100 model from Modern Machine & Tool Co. Inc. as shown in figure 4. The load cell has load limits of 445 N in the axial direction (direction of the flow, x), and 90 N in the normal and lateral (y and z) directions. The load cell is connected to a box converter (figure 4) that converted the strain gauge voltages to axial, normal and side forces, and yaw, roll and pitch moments. A LABVIEW interface was used to display and record the time histories of forces and torques.

Fig. 4. Sting Balance SB-100 (left), signal box converter (right)

The measurements for servo torque are based on the properties of the servo used. As with motor systems, the output torque for the servo was approximated by correlating the input current with the output torque. To find this relationship, calibrations were performed using a microcontroller, PWM Driver, test servo, torque measuring circuit, C++ program, and a MATLAB script to sample and log real-time servo current draw at different applied torques.

The microcontroller used for control and acquisition is a Teensy 3.5 microcontroller. The PWM driver is a PCA965 and is used to control the servo using I2C commands from the Teensy directly. The torque circuit consisted of an analog current sensor (ACS712), bias remover, single pole RC filter, and external 16-bit analog to digital converter (ADS1115). The output torque measurements for the prototype experiments were found by converting the analog voltage output of the torque measuring circuit to servo output torque in N-m using servo torque calibration tests.

2.4 Test Matrix

The input waveform to the flap had the form $\theta(t) = \theta_0 + \theta_A \sin(\omega t)$ with both forebody and tail panel's mean angle of attack set to zero degrees. Here θ_A is the leading edge amplitude of the oscillating tail with respect to the x direction, θ_0 is the tail panel's mean angle of attack and $\omega = 2\pi f$ where f is the forcing oscillatory frequency. Table 1 shows the test cases used to represent the tail of the fish prototype. The dimensions for each panel are expressed as chord length, c by tail Span, S by panel thickness, h.

Table 1. The tail panels used for testing on the fish prototype

Panel	Relative thickness h/c	Dimensions (cm)	Flexural Rigidity β	Mass ratio, μ
a	22.2×10^{-3}	$9 \times 9 \times 0.2$	8.7	0.026
b	1.7×10^{-3}	$9 \times 9 \times 0.015$	2.8	0.004
c	0.8×10^{-3}	$18 \times 9 \times 0.015$	0.3	0.002

The flexural rigidity, β, is a non-dimensional term that represents the tail stiffness and is defined by:

$$\beta = \frac{Eh^3}{12(1-\nu)\rho_f U_{ref}^2 c^3} \tag{1}$$

where U_{ref} is the reference flow velocity relative to the forebody, f is the tail oscillating frequency, c is the chord (panel) length of the tail, h is the thickness of the tail panel, ρ_f is fluid density, and E and ν are the Young's modulus and Poisson ratio of the tail's material respectively. The values of β for the tested panels at freestream velocity of 0.35 m/s are presented in table 1. Based on these values, Tail "a" is termed as the most rigid and tail "c" is termed as the most flexible.

The non-dimensional mass ratio μ (Kim et al., 2013; Connell and Yue, 2007; Alrowaijeh and Hajj, 2018) is defined as:

$$\mu = \frac{\rho_s h}{\rho_f c} \tag{2}$$

Here, ρ_s and ρ_f are the material's and fluid densities respectively. This ratio is the product of the specific gravity ρ_s / ρ_f and effective thickness h/c. The materials used were acrylic for tail 'a' with a density of $1,190$ kg/m^3 and a Young's Modulus of 3.2 GPa, and a carbon fiber for tail panels 'b' and 'c' with a density of $2,276$ kg/m^3 and Young's Modulus of 29 GPa. The tail panel's aspect ratio is the ratio of the panel's span to its chord length, $AR = S/c$. The aspect ratios for panels 'a', 'b' and 'c' are 1, 1 and 0.5 respectively.

The axial force and torque measurements were obtained for two test cases. In case A, the forward speed was set to zero, and all forces and torques generated were due to the acceleration of the panel. Case B included tests performed at a forward speed of 0.35 m/s, and the forces include viscous drag effects. The Reynolds numbers over the tails associated with that speed are 3.5×10^4 for panels 'a' and 'b', and 7.0×10^4 for panel 'c'.

3. RESULTS AND DISCUSSION

Because in case A, the velocity $\bar{U}$ cannot be predetermined, an appropriate scaling parameter for velocity is the tail peak velocity defined by $U_p = 2\pi f A_p$, where A_p is the maximum amplitude of the tip of the tail panel (Kang et al., 2011b; Dewey et al., 2013; Heathcote et al., 2004). The tail's peak to peak amplitude of motion generated by the trailing edge of the panels is a function of system response and is dependent on inertial, elastic and hydrodynamic forces. Peak amplitudes were determined by observing the trailing edge of the panels during the oscillations using a position tracker Matlab script applied to video imagery obtained during the experiment.

3.1 Case A: Measurements Without Towing Speed

Table 2 shows the range of parameters used for testing at zero forward speed. For all results presented in figures 5, 6 and 7, the thrust forces and servo torques increase monotonically with amplitude and frequency with a tendency to flatten at higher forcing frequencies for the lower flexible tails. Tails 'a' and 'b' both generate larger thrusts at higher frequency of oscillations and amplitudes. Figure 7 shows that over the range of tested frequencies, thrust peaks were observed at around 0.7 and 0.8 Hz for all amplitudes for panel 'c'. Thrust peaks occur at lower frequencies for panels with lower flexural rigidity (more flexible). The results may indicate that operating at frequencies arguably close to structural resonance can play a role in achieving thrust peaks. Oscillating the tail near structural resonance can enhance the effect on the coupled elastic, inertia and fluid forces generated by the tail.

Table 2. Range of operating conditions without towing speed

Parameter	**Range**
Free stream velocity, U_∞ (m/s)	0
Frequency of excitation, f (Hz)	$0.5 - 3.0$
Leading edge amplitude, θ_A	6°, 8°, 10°, 12° and 15°
Mean angle of attack, θ_0	0°

Figure 8 shows the relative peak amplitudes A_p for panels 'a', 'b' and 'c' obtained as a result the tail's fluid-elastic response. The peaks were obtained for four successive half strokes, where three trials of A_p measurements were taken for every half a stroke. A maximum peak amplitude typically occurs around the panel's first bending mode in water. Panel 'b' shows an increase in peak amplitudes of 5-40 % higher than rigid panel 'a' in the range of tested frequencies. Maximum peaks for panels 'b' and 'c' were observed at frequencies of 1 Hz and 0.75 Hz respectively. Figure 9 shows a sample of axial force time histories for all tail panels. The responses were generated for the same input of 8 degrees leading edge amplitude, and oscillation frequencies of 1 Hz and 1.5 Hz. Panel 'c' which is the most flexible panel generated at least three times the instantaneous axial forces in comparison to panels 'a' and 'b'. Between panels 'a' and 'b' with the same aspect ratio, both panels generated nearly similar responses in axial force, at least at these tested frequencies. However, panel 'b' begins to generate larger thrust forces at higher frequencies of oscillations (figures 5 and 6).

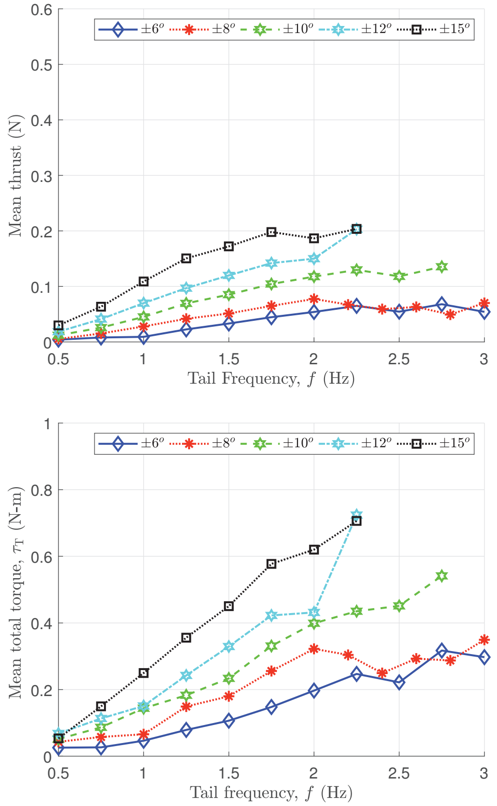

Fig. 5. Thrust (N) and total torque, τ_{T} (N-m) measurements at various leading edge amplitudes and frequencies for tail panel 'a' (most rigid).

Figure 10 shows a comparison of the propulsive efficiency for all panels at zero freestream velocity. The propulsive efficiency is expressed as the Froude efficiency defined by:

$$\eta_{\mathrm{prop}} = \frac{C_{\mathrm{T}}}{C_{\mathrm{P}}} = \frac{TU_{\mathrm{ref}}}{P} \tag{3}$$

where C_{T} and C_{P} are respectively the thrust and power coefficients and expressed as:

$$C_{\mathrm{T}} = \frac{T}{\frac{1}{2}\rho U_{\mathrm{ref}}^2 Sc} \qquad C_{\mathrm{P}} = \frac{P}{\frac{1}{2}\rho U_{\mathrm{ref}}^3 Sc} \tag{4}$$

where T is the mean of the measured thrust (axial force) and P is the mean power input required by the servo to oscillate the panels from the leading edge. Mean power is the mean of the product of the instantaneous hydrodynamic torque, τ_{H} and the tail's prescribed angular velocity ω.

$$P = \overline{\tau_H \omega} \tag{5}$$

The hydrodynamic torque, τ_{H} is obtained by subtracting the servo mechanical torque τ_M from the total servo torque τ_{T}. The mechanical torque τ_{M} is the torque required to move the tailpiece only (without a panel) in the water at all frequency points. In specific, the mechanical torque is the total of mechanical friction and hydrodynamic torque required to move the tailpiece only. The total servo torque is the torque measured at all frequency points in the presence of a tail panel. In equation 5, ω is the angular velocity obtained from the first time derivative of the prescribed simple harmonic motion of the tail panels.

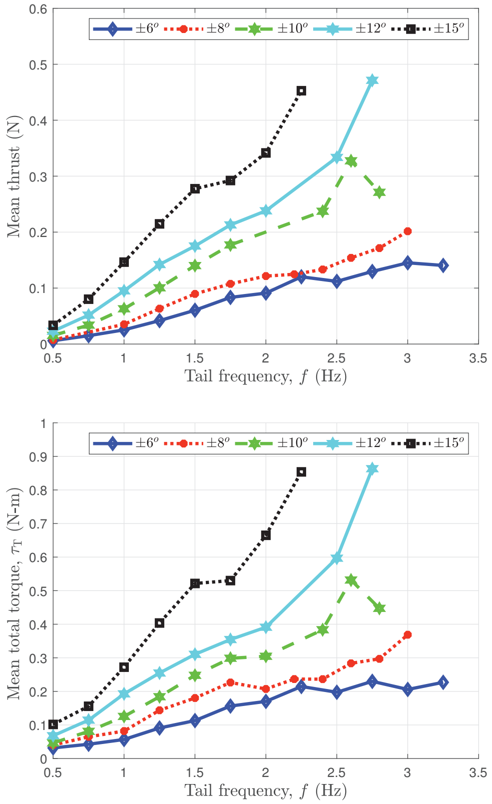

Fig. 6. Thrust (N) and total torque, τ_{T} (N-m) measurements at various leading edge amplitudes and frequencies for tail panel 'b'

The velocity U_{ref} for this set of results is the U_{p} and is obtained using the peak amplitudes presented in figure 8. While results in figure 10 compare propulsive efficiencies for all panels, the scaling approach used here is an appropriate one but not necessarily directly comparable with the propulsive efficiencies obtained for the case with freestream flow; i.e., case B. Although the conventional definition of propulsive efficiency has been used. At zero freestream velocity, another way to measure performance is to use a thrust-to-power-input ratio (Heathcote et al., 2004). The results in figure 10 show that the thrust-power input ratio is greater for the flexible panels than for the rigid panel

3.2 Case B: Measurements With Towing Speed

In this subsection, forces and torques were measured and recorded when the prototype was towed at a speed of 0.35 m/s. Table 3 shows the range of input parameters used for this test condition. In the case of forward speed, the net thrust force is the force generated due to the addition of flow circulation, and viscous body drag. The thrust force, T generated due to these effects was determined by taring the static body drag measured when the prototype was towed unactuated, D_{body}, from the net thrust force obtained from direct force measurements when actuated and towed, T_{net}.

$$T = T_{\mathrm{net}} - D_{\mathrm{body}} \tag{6}$$

Figure 11 shows the true body drag values generated by towing the prototype (unactuated) at three different

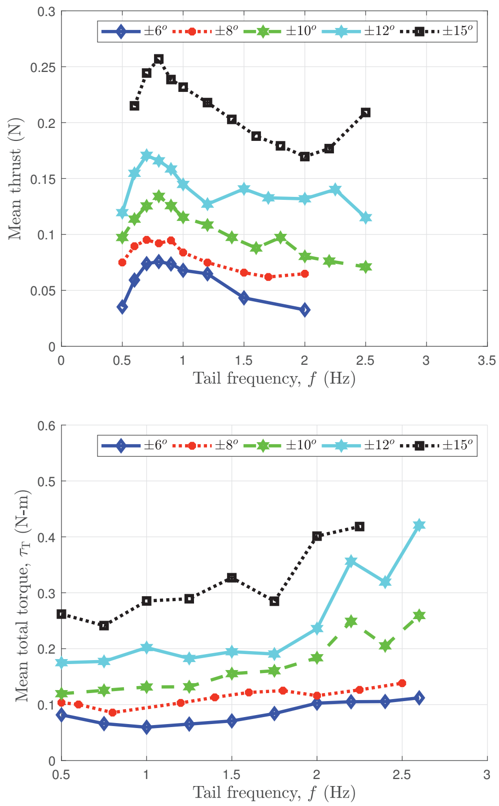

Fig. 7. Thrust (N) and total torque, τ_{T} (N-m) measurements at various leading edge amplitudes and frequencies for tail panel ’c’ (most flexible).

Table 3. Range of operating conditions with towing speed

Parameter	**Range**
Free stream velocity, U_∞ (m/s)	0.35
Frequency of excitation, f (Hz)	$0.5 - 3$
Leading edge amplitude, θ_A	8°
Tail’s mean angle of attack, θ_0	0°

freestream velocities. The drag forces have a quadratic relationship with flow velocity, and are directly proportional to the velocity squared, a behavior typically expected. The drag coefficients of the forebody at the three nonzero speeds are 0.062, 0.059 and 0.063 respectively. The averaged drag coefficient over the three speeds is 0.061.

Two additional non-dimensional frequency parameters are introduced. These are the reduced frequency, k, and Strouhal number St :

$$k = \frac{2\pi f c}{U_{\text{ref}}} \quad \text{and} \quad St = \frac{f A_{\text{p}}}{U_{\text{ref}}} \tag{7}$$

where, A_{p} is the peak amplitude which is the recommended scaling parameter extensively used by literature. Since Strouhal number is an output response of the system, the results are presented as a function of reduced frequency.

The coupling effects between aspect ratio and stiffness on propulsive performance can be isolated in these set of results. Panels ’a’ and ’b’ have the same aspect ratio and only vary in material type and hence flexibility, whereas panels ’b’ and ’c’ are the same material, but vary in aspect ratio. Figure 12 shows that at higher reduced frequencies, tail panels ’a’ and ’b’ generated higher thrust coefficient values than panel ’c’. However, for the range of reduced frequency between k =3.5 and k =5, panel ’c’ generated higher dimensional thrust forces prior to converting the results to non-dimensional form. Out of the three tail panels, panel ’c’ panel ’c’ also required the least amount of power input into the fluid to generate the flapping motion.

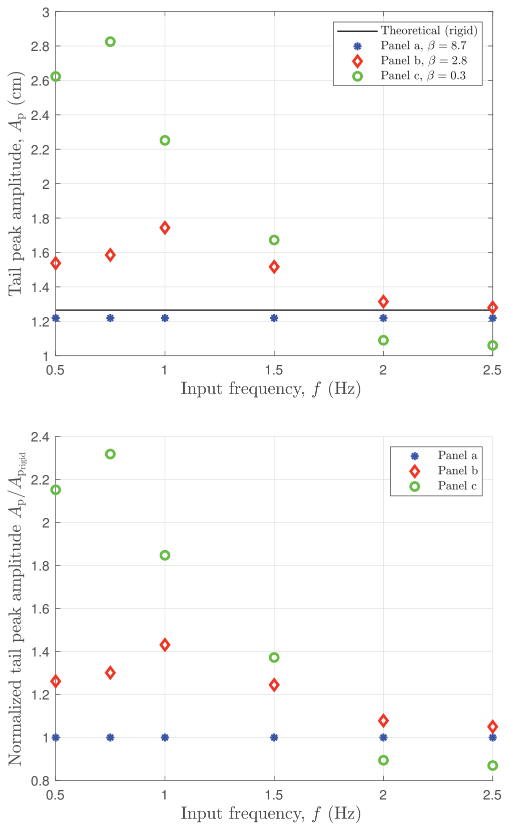

Fig. 8. Dimensional peak amplitude (top) and normalized peak amplitudes (bottom)

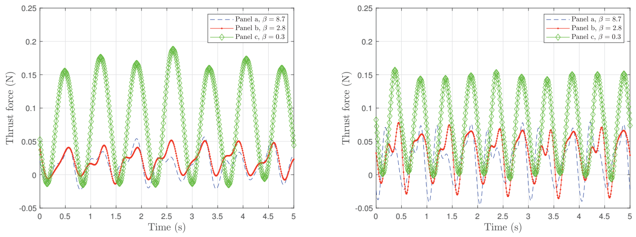

Fig. 9. Time series for instantaneous thrust force for frequency of oscillation of 1 Hz (left) and 1.5 Hz (right). Panel ’a’: blue dashed, panel ’b’: solid red, panel ’c’: green star,

When directly comparing tail panels ’a’ and ’b’, panel ’b’ generated higher thrust forces for nearly the same servo torque requirements. At reduced frequencies beyond $k = 4$, it is clear that some degree of the fluid-elastic response exhibited by panel ’b’ enhances thrust production.

Optimal propulsive performance is generally expected over a band of frequency where the flow exhibit favorable vortex

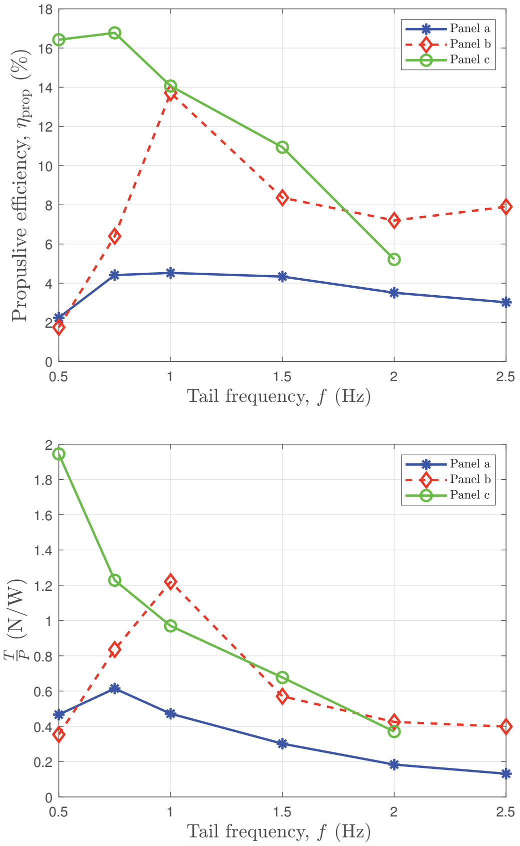

Fig. 10. Propuslive efficiency peaks (top) and thrust to power ratio (bottom) for all three panels for case A. Panel 'a': blue star panel 'b': red diamond, panel 'c': green circle,

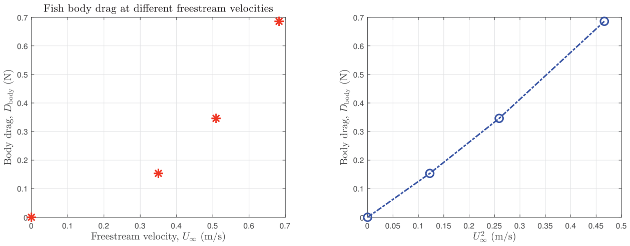

Fig. 11. Body drag force vs freestream velocity

behavior to the benefit of thrust production. Figure 14 compares the propulsive efficiency curves for all three tail panels. Tail panel 'c' shows propulsive efficiencies up to 45%, nearly a 280% increase in value relative to panel 'b'. Panel 'b' is nearly eight times the flexural rigidity of panel 'c', and panel 'a' is nearly three times the flexural rigidity of panel 'b'. While panels 'a' and 'b' maintain the same aspect ratio and only differ in material property, tail 'b' was able to generate about 35% increase in propulsive efficiency. The results show that flexibility enhances propulsive efficiency, although both geometric and material properties tend to have different effects at different operating frequencies. Figure 14 also shows that the maximum peaks were observed at a range reduced frequency somewhere between $k = 4$ and $k = 5$ for tail panels 'b' and 'c', and at lower reduced frequency of $k = 3.8$ for tail panel 'a'. The propulsive efficiency peaks

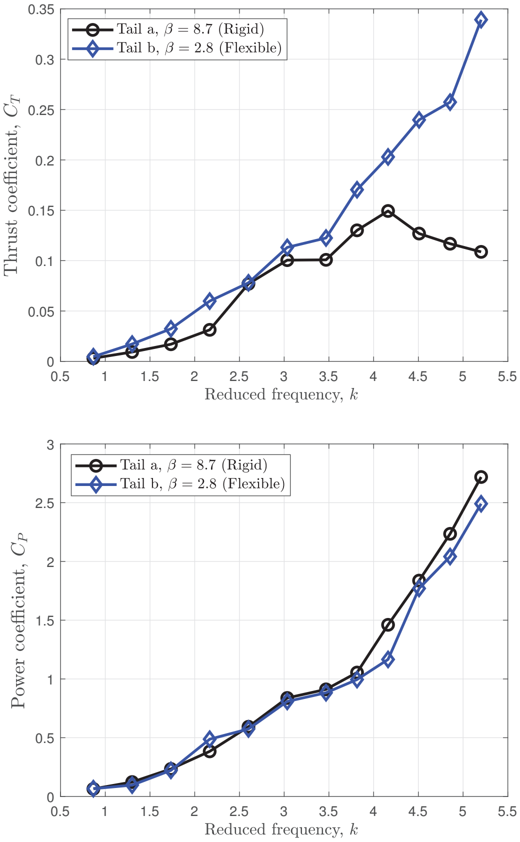

Fig. 12. Thrust and power coefficients for tail panels 'a' and 'b'

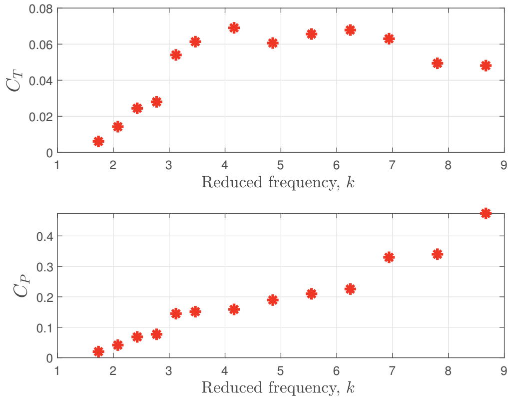

Fig. 13. Thrust and power coefficients for tail panel 'c'

presented by Dewey et al are observed at around $k = 6$ to 7 for panels P_4 and P_5 with flexural rigidity values close to our panel 'b'. The difference in results is due to some governing factors the biggest one of them is regime flow, where Dewey et al. presented their results at a Reynolds number of Re=7,200. Reynolds number can have drastic effects on skin friction and pressure drag acting on the panel which as a result can alter thrust generation and power input to the fluid by the panels.

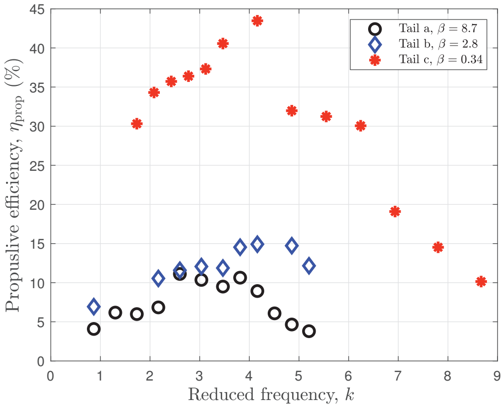

Fig. 14. Full comparison of propulsive efficiencies

4. CONCLUSION

A single link swimming device has been designed, fabricated and tested in a towing basin. The results show that for the same oscillatory amplitudes and flow speed, an increase in frequency of oscillations results in a monotonic increase in thrust coefficients up to a peak frequency. This behavior is the same regardless of tail material flexibility.

At zero forward speed, propulsive peaks showed significant differences between three panels. Panel 'c' produced 59% higher maximum propulsive efficiency values than panel 'b' (varying aspect ratio). Panel 'b' produced 98% higher maximum propulsive efficiency values than panel 'a' (varying material property).

At a speed of 0.35 m/s, the propulsive efficiency is more affected by changes in geometric properties (aspect ratio) rather than material properties. The results show that by incorporating three times the flexibility on rigid tail, panel 'a', the propulsive efficiency was enhanced by 35%. In addition, incorporating eight times the flexibility on panel 'b' resulted in panel 'c' generating approximately 280% increase in propulsive efficiency. Increasing the material's flexibility tends to shift the propulsive peaks to higher reduced frequencies. Isolating the effects of aspect ratio, lowering the aspect ratio for the same material generated larger differences in propulsive efficiency peaks, but produced no notable shift in efficiency peaks to a different frequency. Finally, it is determined that the overall flexibility of a material provides better peak propulsive efficiency values.

ACKNOWLEDGEMENTS

The authors kindly acknowledge the support of the National Science Foundation (NSF) under the Grant No. CMMI-1635143. The authors also gratefully acknowledge the help provided by the following undergraduate research assistants: Ahmed Nayfeh, Alex Mclean, Charles Watson, Colton Beardsley, Khanh Nguyen, and Luke Bergeron.

REFERENCES

Alrowaijeh, J.S. and Hajj, M.R. (2018). Piezoelectric energy harvesting from flexible delta wings. *Theoretical and Applied Mechanics Letters*, 8(4), 267–271.

Anderson, J., Streitlien, K., Barrett, D., and Triantafyllou, M. (1998). Oscillating foils of high propulsive efficiency. *Journal of Fluid Mechanics*, 360, 41–72.

Connell, B.S. and Yue, D.K. (2007). Flapping dynamics of a flag in a uniform stream. *Journal of fluid mechanics*, 581, 33–67.

Dewey, P.A., Boschitsch, B.M., Moored, K.W., Stone, H.A., and Smits, A.J. (2013). Scaling laws for the thrust production of flexible pitching panels. *Journal of Fluid Mechanics*, 732, 29–46.

Eloy, C. (2012). Optimal strouhal number for swimming animals. *Journal of Fluids and Structures*, 30, 205–218.

Ghommem, M., Hajj, M.R., Beran, P.S., and Puri, I.K. (2014). Role of wing morphing in thrust generation. *Theoretical and Applied Mechanics Letters*, 4(3), 032003.

Heathcote, S., Martin, D., and Gursul, I. (2004). Flexible flapping airfoil propulsion at zero freestream velocity. *AIAA journal*, 42(11), 2196–2204.

Heathcote, S. and Gursul, I. (2007). Flexible flapping airfoil propulsion at low reynolds numbers. *AIAA journal*, 45(5), 1066–1079.

Kang, C.K., Aono, H., Cesnik, C.E., and Shyy, W. (2011a). Effects of flexibility on the aerodynamic performance of flapping wings. *Journal of fluid mechanics*, 689, 32–74.

Kang, C.K., Aono, H., Cesnik, C., and Shyy, W. (2011b). A scaling parameter for the thrust generation of flapping flexible wings. In *49th AIAA Aerospace Sciences Meeting Including the New Horizons Forum and Aerospace Exposition*, 1313.

Kim, D., Cossé, J., Cerdeira, C.H., and Gharib, M. (2013). Flapping dynamics of an inverted flag. *Journal of Fluid Mechanics*, 736.

Koochesfahani., M. (1989). Vortical patterns in the wake of an oscillating airfoil. *AIAA Journal*, 27(9).

Lauder, G.V. and Madden, P.G. (2007). Fish locomotion: kinematics and hydrodynamics of flexible foil-like fins. *Experiments in Fluids*, 43(5), 641–653.

Prempraneerach, P., Hover, F., and Triantafyllou, M.S. (2003). The effect of chordwise flexibility on the thrust and efficiency of a flapping foil. In *Proc. 13th Int. Symp. on Unmanned Untethered Submersible Technology: special session on bioengineering research related to autonomous underwater vehicles, New Hampshire*, volume 152, 152–170.

Quinn, D.B., Lauder, G.V., and Smits, A.J. (2014). Scaling the propulsive performance of heaving flexible panels. *Journal of fluid mechanics*, 738, 250–267.

Shyy, W., Ifju, P., and Viieru, D. (2005). Membrane wing-based micro air vehicles. *Applied mechanics reviews*, 58(4), 283–301.

Triantafyllou, G.S., Triantafyllou, M., and Grosenbaugh, M. (1993). Optimal thrust development in oscillating foils with application to fish propulsion. *Journal of Fluids and Structures*, 7(2), 205–224.

Triantafyllou, M., Triantafyllou, G., and Gopalkrishnan, R. (1991). Wake mechanics for thrust generation in oscillating foils. *Physics of Fluids A: Fluid Dynamics*, 3(12), 2835–2837.